

Supplemental Information

DNA substrates

PAGE-purified DNA substrates were purchased from Bioneer Co. (Daejeon, Korea). For crystallization, DNA molecules were further purified and annealed. Crystal I of the DNA substrate contained 5'-GAATGTGTGTCTCAATCCCAAC-3', 5'-GTTGGGATTG-3', and 5'-AACCAGACACACATTTC-3'. The various DNA substrates for the nuclease assay summarize in the Figure S8. 5'-³²P-labeled substrates were prepared with Poly nucleotide kinase (Roche Applied Science, Rockford, IL, USA) and γ -³²P-dATP (PerkinElmer, Waltham, MA, USA). 3'-³²P-labeled substrates were prepared with Terminal transferase (Roche Applied Science, Rockford, IL, USA) and α -³²P-dATP (PerkinElmer, Waltham, MA, USA). The substrates were annealed in buffer containing 150 mM NaCl and, 15 mM sodium citrate buffer, boiled at 95°C for, 5 min, and then allowed to cool for overnight.

Mutagenesis

All the *PaFAN1* mutants used in this study were created by PCR-based methods (Stratagene). The mutant proteins were purified using affinity chromatography followed by Resource-Q as described above. Val191 and Leu192 (wedge mutant) were simultaneously mutated to arginine, and Val191, Leu192, Leu195 and Ile197 were simultaneously mutated to alanine. Tyr21, Trp184, and Ile197 (NTD mutant) were mutated to alanine, respectively. Arg65 and Arg333 (DNA binding mutant) were mutated to tyrosine and glutamic acid, respectively. Arg65 and Arg69 were simultaneously mutated to alanine. Trp253 and Leu421 (bowl mutant) were mutated to proline and arginine, respectively. Asp528 and Gln534 (active site mutant) were mutated to alanine, respectively. All the *SpFAN1* mutants used in this study were created by PCR-based methods (Stratagene). Arg103 and Arg107 were simultaneously mutated to alanine. Ile257 and Leu258 were simultaneously mutated to arginine. Ala360 and Leu564 were mutated to proline and arginine, respectively. Gln678 was mutated to alanine. The quadruple and N-term truncation mutants were derived from Fontebasso et al, 2013.

Supplementary figure legends

Supplemental Figure 1. Sequence alignment of PaFAN1.

Structure-based sequence alignment of FAN1 nuclease family members. The organisms are *Pseudomonas aeruginosa* (Uniprot ID, PQ9I2N0), *Comamonas testosteroni* (D0IVN7), *Achromobacter arsenitoxydans* (H0F0Z9), *Halomonas elongata* (E1V9B7), *Gallaecimonas xiamenensis* (K2K2K5), *Vibrio orientalis* (C9QFT8), *Arabidopsis thaliana* (Q9SX69), *Oryza sativa* (B9FRR6), *Mus musculus* (Q69ZT1), *Danio rerio* (Q1LWH4), *Caenorhabditis elegans* (P90740), *Schizosaccharomyces pombe* (Q9Y804), *Homo sapiens* (Q9Y2M0). Strictly conserved and highly conserved residues are highlighted in orange and yellow, respectively. Every 10th residue is marked with a black dot. FAN1 residues mutated in this study are highlighted with a purple circle. Functionally important residues are indicated: conserved residues in the active site, blue stars; DNA-binding residues, red triangles; hydrophobic wedge, blue open circle. Sequence alignment was performed using Clustal X (Larkin et al. 2007).

Supplemental Figure 2. Biochemical characterization of PaFAN1.

(A) Endonuclease activity of PaFAN1 in the presence of Mn²⁺ or Mg²⁺ ions. The cleavage reaction solution containing 5' flap DNA substrate (20 nM) and various amounts of PaFAN1 (100, 200, 400 nM) was incubated for 30 min at 37°C. The 5'-³²P-label is marked with a filled circle. (B) Endonuclease activity analysis for the 3'-³²P-labeled 5' flap DNA substrate. The reaction conditions are the same as those of S2A. The ³²P-label is marked with a filled circle. (C) Endonuclease activity of PaFAN1 in the presence of Mn²⁺ ions. The reaction solution containing the 5' flap DNA substrate (10 nM) and PaFAN1 (50 nM) was incubated for 30 or 60 min at 37°C.

Supplemental Figure 3. The interface at the NTD, TPR, and VRR nuc domains forms a pocket that houses the 5' flap.

(A) The intervening omega loop (α 10- α 11) of the NTD and the TPR domain (blue)

encloses half of an omega loop of the VRR domain ($\alpha 19$ - $\alpha 20$, pink) in a perpendicular manner. For clarity, DNA is omitted. A central hole is marked. At the bottom left, a cartoon is shown for the simple view. (B) Surface representation of the interface of the pocket with 5' flap DNA. The figure is in the same orientation as that of Supplemental Fig. 3A. (C) A 90° rotated view of Supplemental Fig. 3A. Residues forming the pocket are shown in yellow sticks. For clarity, DNA is omitted. On the top right, a scheme is shown for the simple view. (D) Surface representation of the interface of the pocket with 5' flap DNA. The figure is in the same orientation as that of Supplemental Fig. 3C. The 3.2 Å *PaFAN1*-DNA structure was used in Supplemental Figs. 3A-3D, 4A, 4B, and 5A.

Supplemental Figure 4. Structures of the individual domain of *PaFAN1*.

(A) Overall structure of the NTD and SAP domains. Two β -sheets (($\beta 1/\beta 5$ from NTD) and ($\beta 3/\beta 4$ from SAP)) make a head-to-tail interface, forming an L-shaped turn to facilitate accommodation of the pre-nick segment within the two domains. DNA-contacting residues are marked with red spheres. (B) Overall structure of the TPR domain. The two inner helices $\alpha 15$ and $\alpha 17$ are tilted relative to the first two helices $\alpha 11$ and $\alpha 13$, resulting in a slightly concave shape that allows all four helices to participate in recognition of the post-nick duplex. (C) Structure of the VRR nuc domain of *PaFAN1*. The catalytic sub-domain is shown in magenta and the six-helix bundle is shown in gold. Mn^{2+} ions are shown in yellow spheres. (D-F) Comparison of the topologies of *PaFAN1*, *PfHjc*, and phage (*Streptococcus equi*) single domain VRR nuclease (4QBO). Topologically similar parts are boxed.

Supplemental Figure 5. Electron density map for DNA complexed with FAN1.

(A) A 3.2 Å simulated annealed *2Fo-Fc* omit map (1.0 σ) of the metal-free *PaFAN1*-DNA showing pre-nick DNA bound to the NTD and SAP domain. The nicked end of a pre-nick segment is blocked by the $\alpha 10$ wedge helix and makes a sharp kink at the C13 and T12 of the template strand. (B) A *Fo-Fc* difference map (3.5 σ)

for a metal ion is shown at 4.0 Å resolution. The map was calculated with phases after molecular replacement using the metal-free *Pa*FAN1-5'DNA complex as a search model.

Supplemental Figure 6. Nuclease activity of various FAN1 proteins on 5' flap DNA.

(A) Nuclease activities of various FAN1 mutants on 5' flap DNA were examined in the presence of Mn^{2+} ion. Proteins (50 nM) were added to 5' flap DNA (10 nM) at 37°C for 10 or 30 sec. (B) Nuclease activities of various FAN1 mutants on 5' flap DNA were examined in the presence of Mn^{2+} ion for 1 or 5 min. Assay conditions are same as those in Supp. Fig. 6A. (C) Nuclease activities of various FAN1 mutants on 5' flap DNA were examined in the presence of Mg^{2+} ion. Proteins (50 nM) were added to 5' flap DNA (10 nM) at 37°C for 1 or 5 min. (D) The percentage of the cleaved DNA substrate after the reaction in Supp. Figure 6C was quantified using phosphorimager analysis. The error bars are calculated from the standard deviation.

Supplemental Figure 7. Metal-induced conformational change in the 5' flap DNA bound to FAN1.

(A, B) Structural comparison of a portion of the post-nick duplex bound to the VRR nuc domain in the absence (A) and presence (B) of Mn^{2+} ions. (C, D) A portion of the pre-nick duplex bound to the VRR nuc domain in the absence (C) and presence (D) of the Mn^{2+} ion. A simulated annealed omit $2Fo-Fc$ map (0.9σ) is shown at the bottom of each figure. (E, F) Structural comparison of the 5' flap region bound to the pocket in the absence (E) and presence (F) of the Mn^{2+} ion. The model is shown with the simulated annealed omit $Fo-Fc$ map (2.8σ). The maps were calculated at 3.2 Å for 7A, C, E, and at 4.0 Å for 7B, D, F.

Supplemental Figure 8. Structures of the substrates used in this study.

Structures of the substrates used in this work. (A-D) 5' flap DNA substrates with various gaps, (E, F) RF and a modified RF DNA, (G) 3' flap DNA, (H) splayed-arm DNA, (I) dsDNA with a 5' overhang, (J) nicked DNA, (K) nicked HJ, (L) dsDNA, (M) HJ DNA, and (N) 5' flap DNA for Fig 6C.

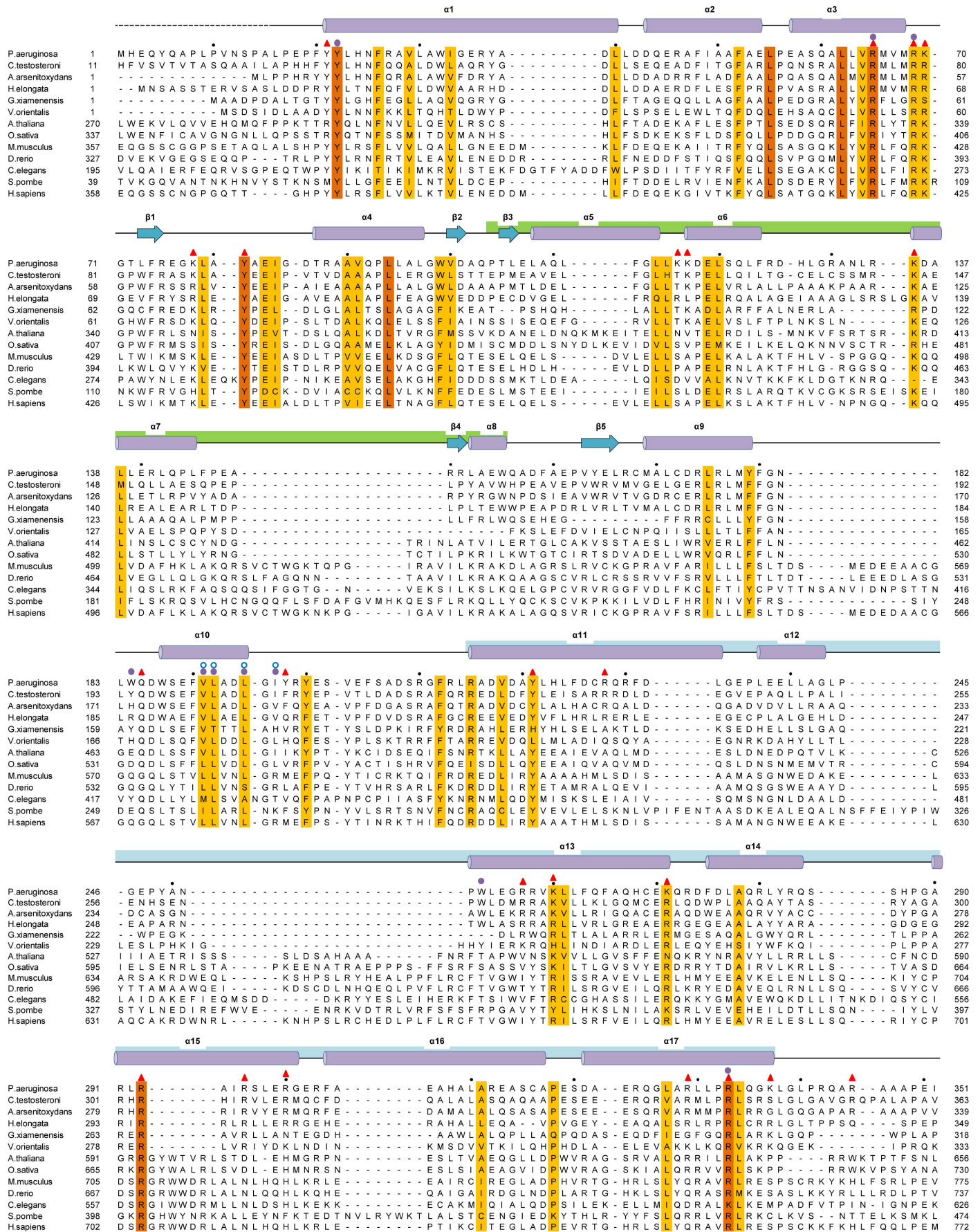
Supplemental Movie 1. Overall structure, four domains, and an active site of *PaFAN1* bound to 5' flap DNA.

Overall structure of the *PaFAN1*-5' flap DNA structure is shown in various angles.

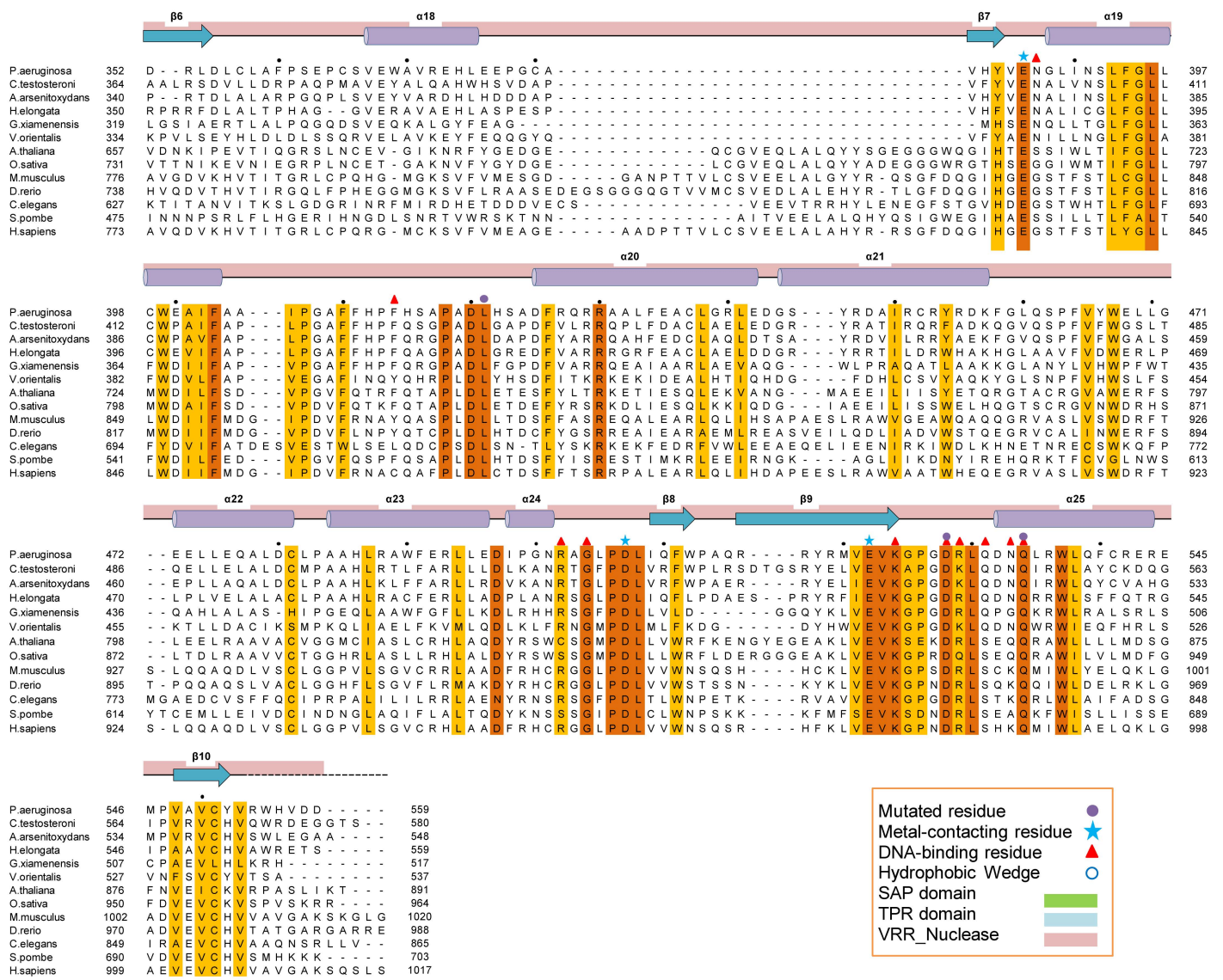
Supplemental Movie 2. Clamping motion of *PaFAN1* facilitates the incision of a substrate.

Supplemental References

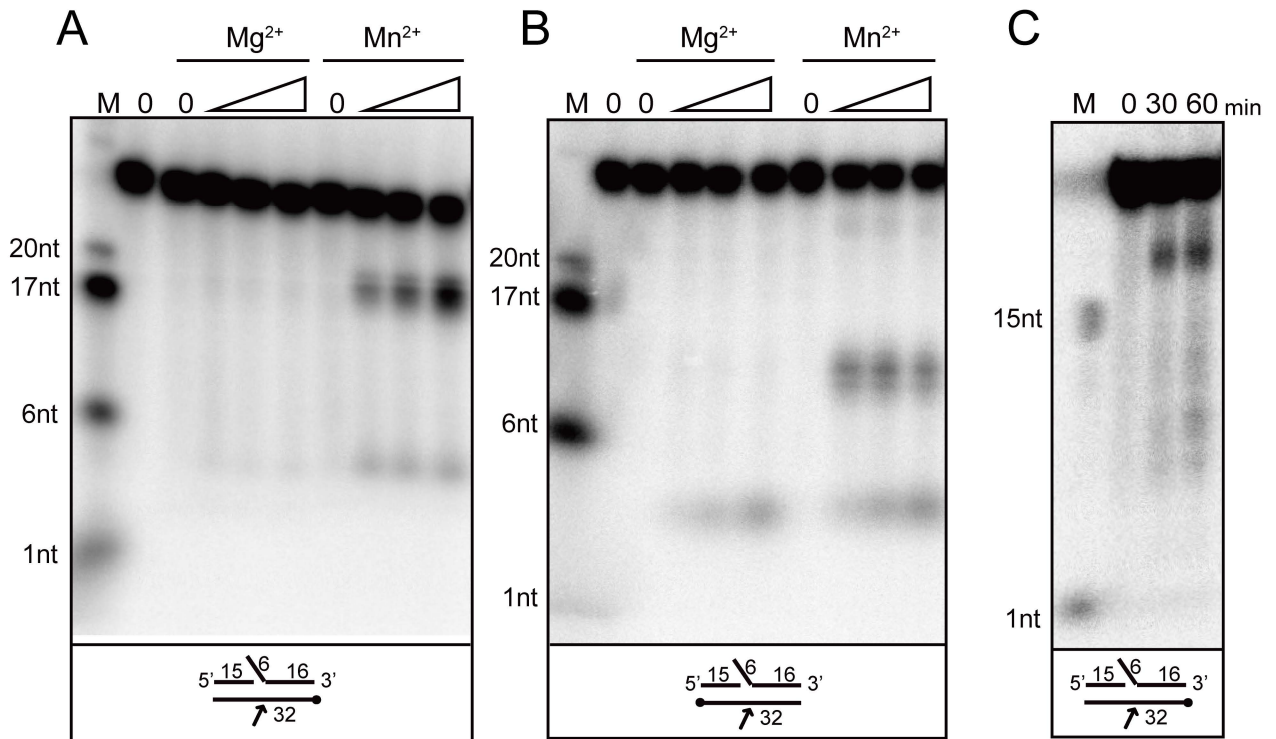
Larkin, MA., Blackshields, G., Brown, NP., Chenna, R., McGettigan, PA., McWilliam, H., Valentin, F., Wallace, IM., Wilm, A., Lopez, R., et al. 2007. Clustal W and Clustal X version 2.0. *Bioinformatics* **23**: 2947-2948

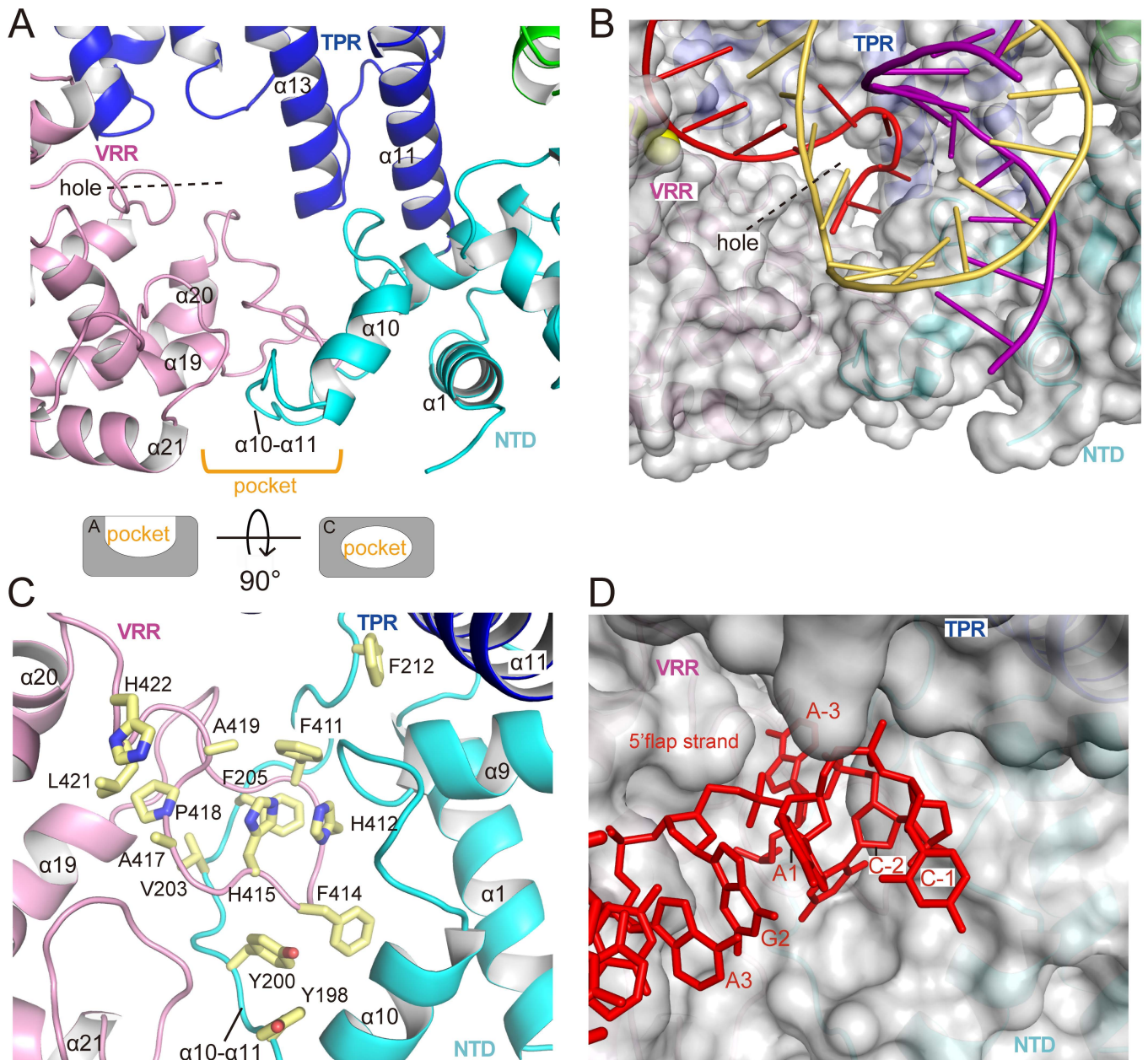


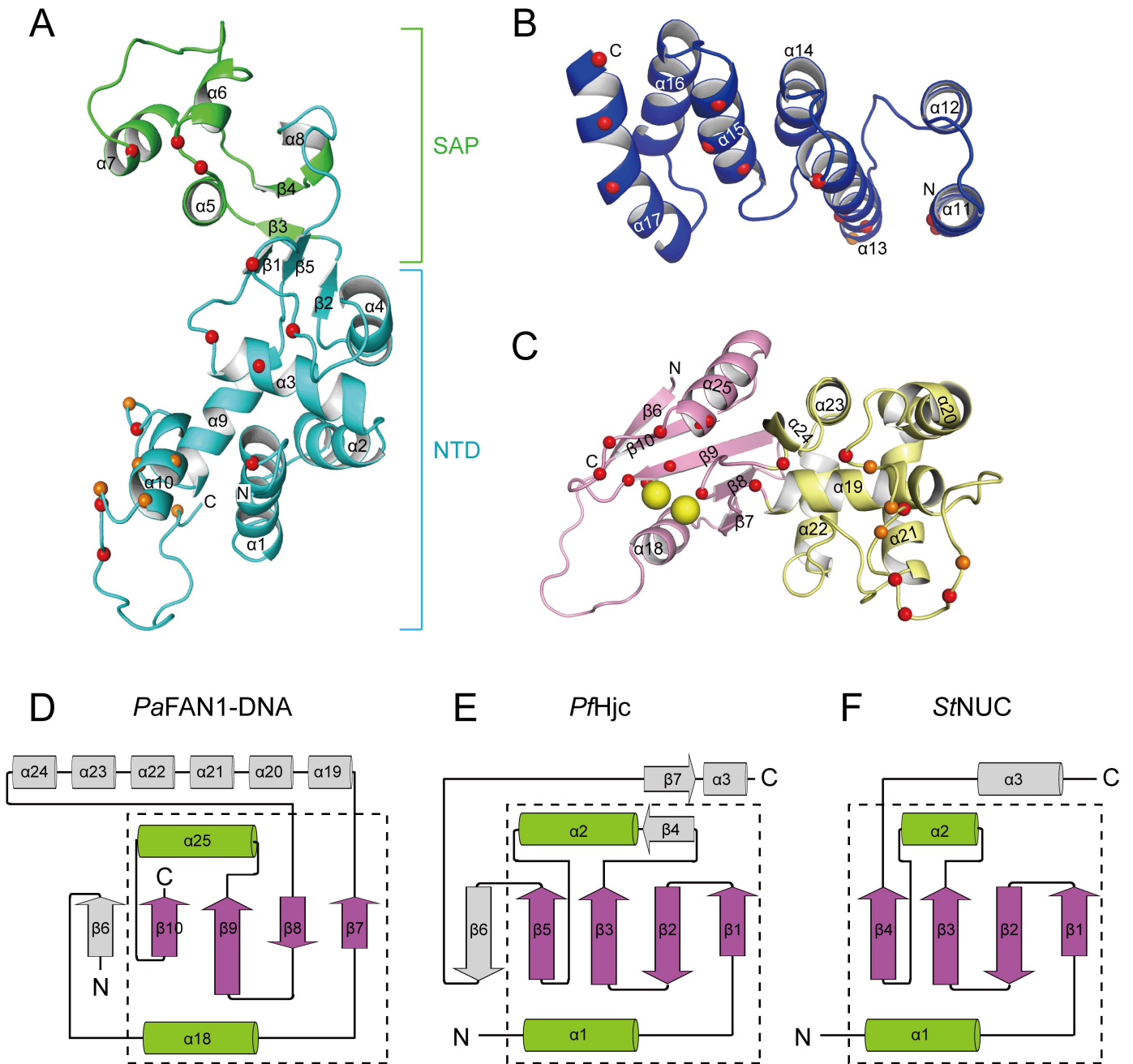
Supplemental Figure 1

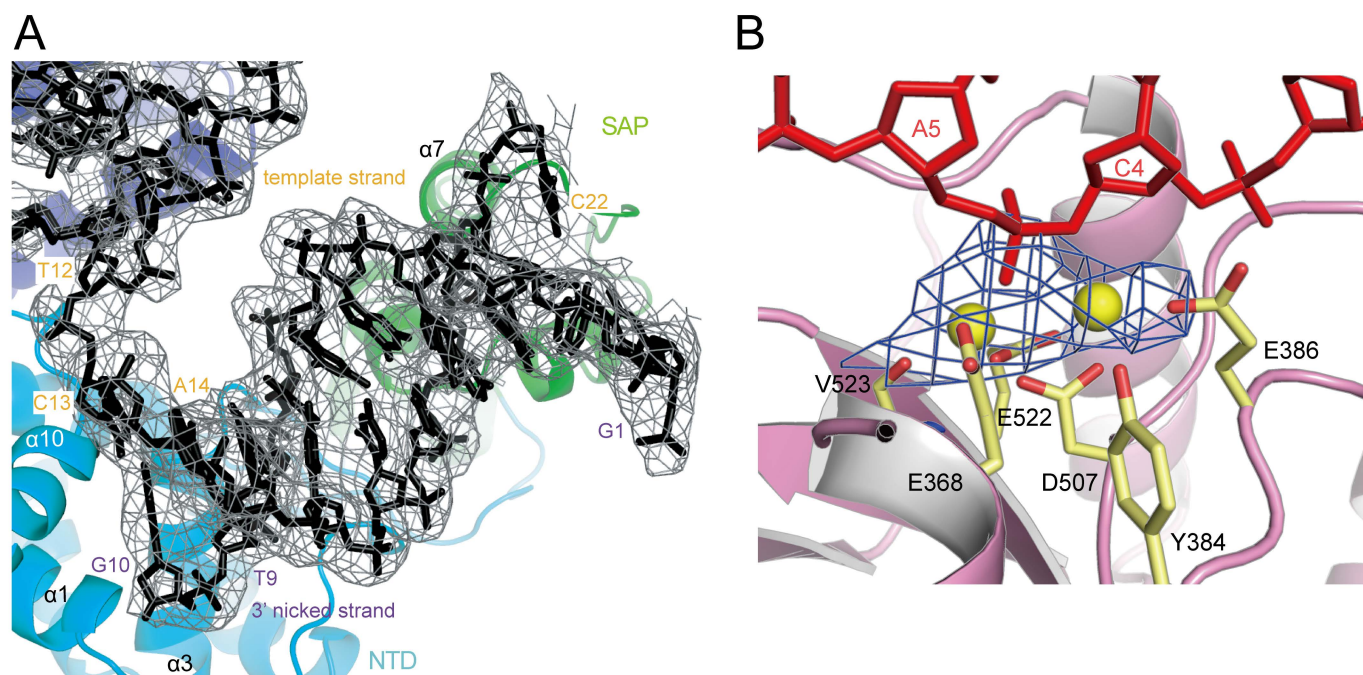


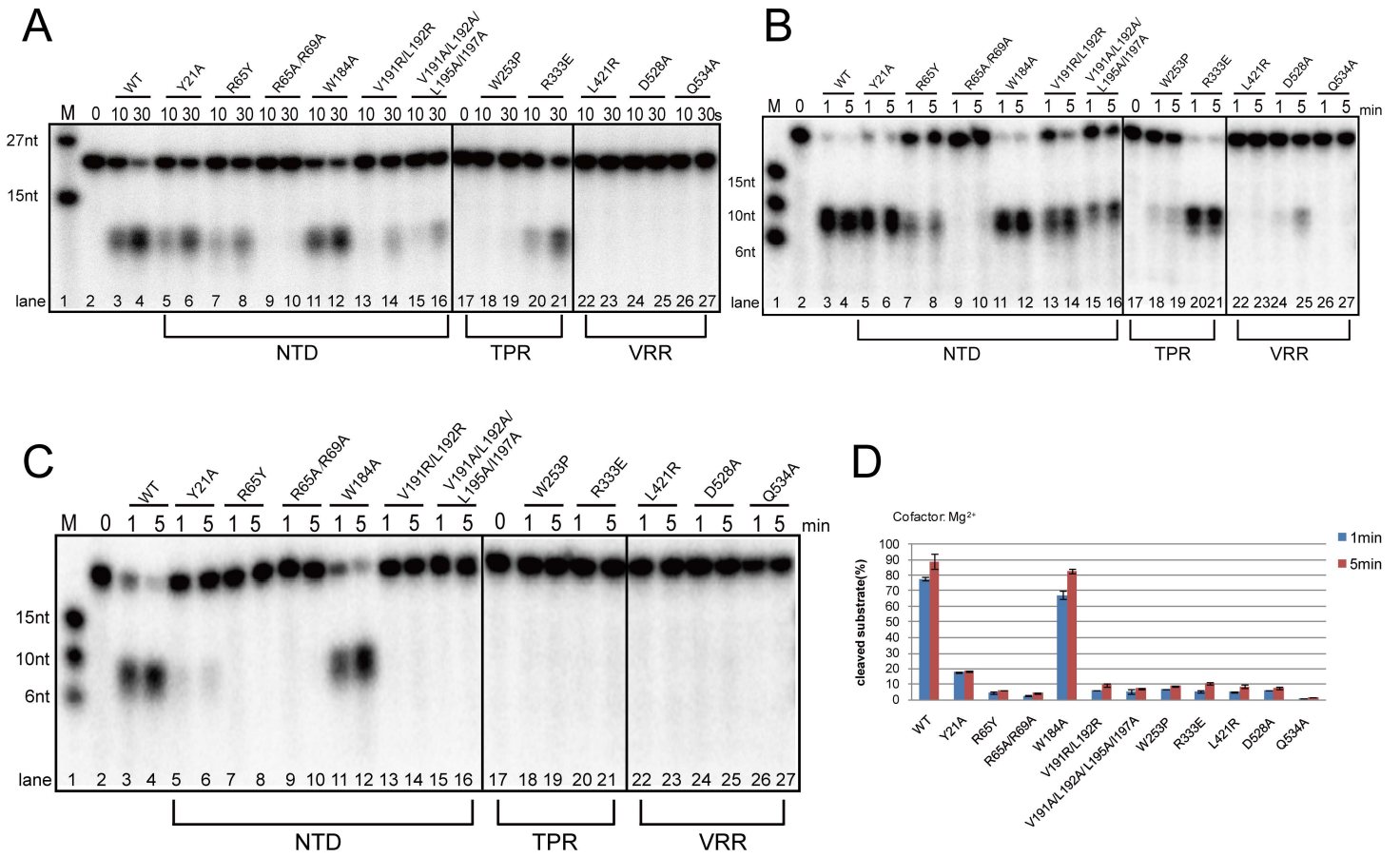
Supplemental Figure 1



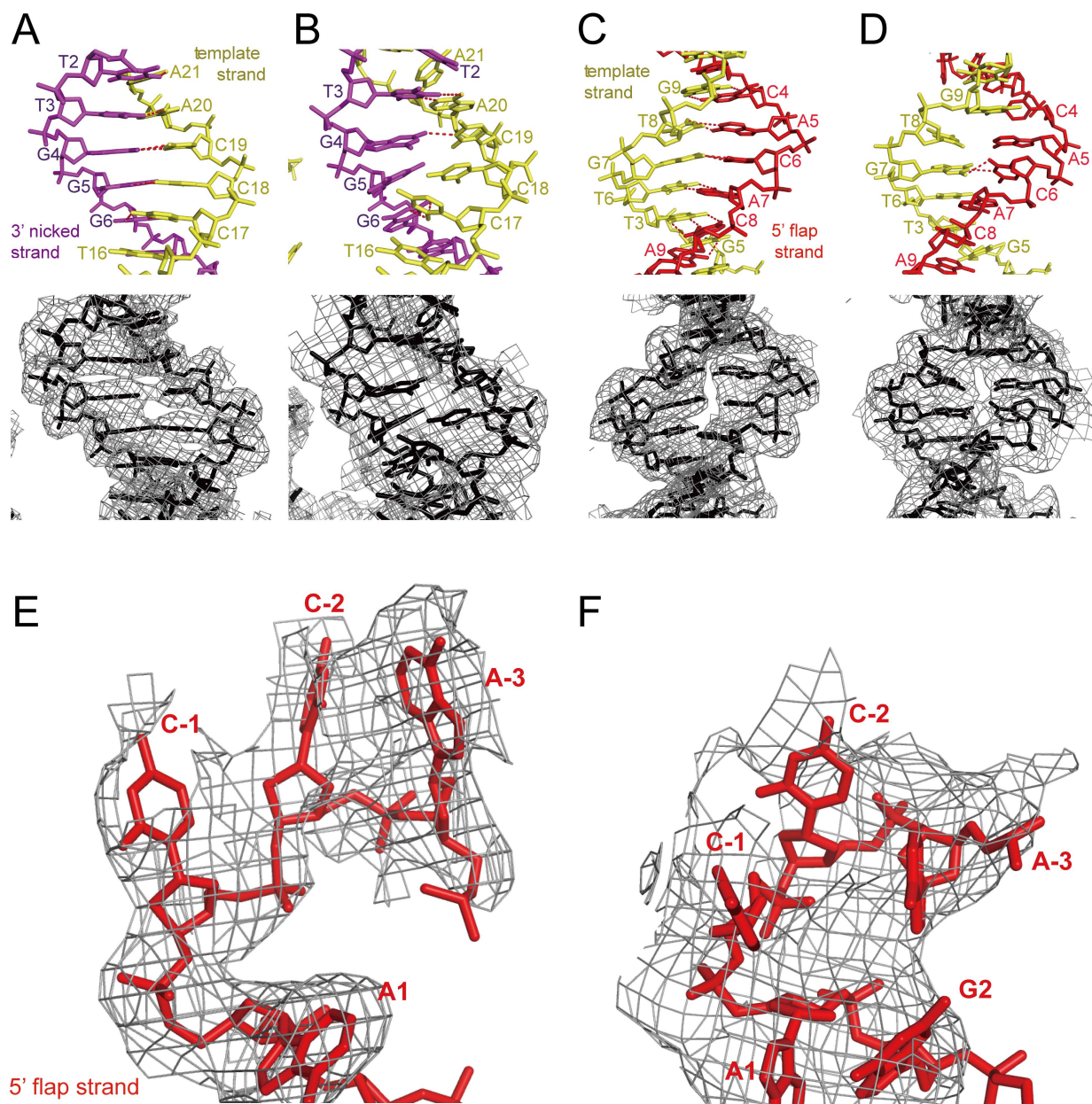








Supplemental Figure 6



Supplemental Table 1. Data collection and refinement statistics

	Sel-Met	Native	Mn ²⁺ soaking
Data collection			
Space group	P2 ₁	P2 ₁	P2 ₁
Cell dimensions			
<i>a</i> , <i>b</i> , <i>c</i> (Å)	80.2, 105.9, 107.1	76.6, 106.7, 142.2	81.1, 106.9, 107.5
α , β , γ (°)	90, 89.98, 90	90, 89.97, 90	90, 89.8, 90
Resolution (Å)	50-3.26(3.31-3.26) ¹	50-3.17(3.23-3.17)	50-4.00(4.07-4.00)
R _{sym} (%) ²	10.2(87.6)	8.0(88.5)	10.8(84.0)
<i>I</i> / σ	17.7(1.9)	30.5(3.1)	19.0(2.3)
Completeness (%)	99.2(98.2)	99.8(100.0)	99.7(99.6)
Redundancy	3.6(3.6)	7.1(7.1)	4.6(4.4)
Overall Figure of merit (33-3.2 Å)	0.44		
Refinement			
Resolution (Å)		32.2-3.2	44.6-4.0
No. reflections		37835	15461
R _{work} /R _{free} (%) ³		19.5/23.4	22.4/27.8
No. atoms			
Protein		8766	8750
DNA/Mn ²⁺		1884	1922/4
Water		2	
B-factors			
Protein		113.9	146.9
DNA/Mn ²⁺		137.8	166.0/100.8
Water		88.1	
R.m.s deviations			
Bond lengths (Å)		0.003	0.004
Bond angles (°)		0.872	0.910
Ramachandran Plot			
Most favored(%)		95.0	89.9
Allowed(%)		5.0	9.5
Outlier(%)		0	0.6
Clashscore		16.8	2.8

¹Values in parentheses are for the highest shell. ² $R_{sym} = \sum_h \sum_i |I_{h,i} - I_h| / \sum_h \sum_i I_{h,i}$, where I_h is the mean intensity of the i observations of symmetry related reflections of h . ³ $R = |F_{obs} - F_{calc}| / F_{obs}$, where $F_{obs} = F_{pi}$ and F_{calc} is the calculated protein structure factor from the atomic model (R_{free} was calculated with 5% of the reflections). R.m.s deviation in bond lengths and angles are the deviations from ideal values, and the r.m.s. deviation in B factors is calculated between bonded atom.

Supplemental Table 2. *S. pombe* strains used in this study

Strain code	Genotype
AMC501	<i>h-</i> , <i>ura4D18</i> , <i>leu1-32</i> , <i>ade6-704</i>
SAL161	<i>h-</i> , <i>rad3::kanMX6</i> <i>ade6-704</i> , <i>leu1-32</i> , <i>ura4-D18</i>
YFS228	<i>h+</i> , <i>fan1::loxP-ura4+-loxM3</i> , <i>pso2::kanMX6</i> , <i>ura4D18</i> , <i>leu1-32</i> , <i>ade6-704</i>
YFS302	<i>h-</i> , <i>fan1::loxP-natMX6-loxM3</i> , <i>pso2::kanMX6</i> , <i>ura4D18</i> , <i>leu1-32</i> , <i>ade6-704</i>
YFS309	<i>h+</i> , <i>loxP-fan1-R160E/R164E/K171E/R173E-loxM3</i> , <i>pso2::kanMX6</i> , <i>ura4D18</i> , <i>leu1-32</i> , <i>ade6-704</i>
YFS310	<i>h+</i> , <i>loxP-fan1-1-193Δ-loxM3</i> , <i>pso2::kanMX6</i> , <i>ura4D18</i> , <i>leu1-32</i> , <i>ade6-704</i>
AW994	<i>h+</i> , <i>loxP-fan1-R103A/R107-loxM3</i> , <i>pso2::kanMX6</i> , <i>ura4D18</i> , <i>leu1-32</i> , <i>ade6-704</i>
AW996	<i>h+</i> , <i>loxP-fan1-I257R/L258R-loxM3</i> , <i>pso2::kanMX6</i> , <i>ura4D18</i> , <i>leu1-32</i> , <i>ade6-704</i>
AW998	<i>h+</i> , <i>loxP-fan1-A360P-loxM3</i> , <i>pso2::kanMX6</i> , <i>ura4D18</i> , <i>leu1-32</i> , <i>ade6-704</i>
AW1000	<i>h+</i> , <i>loxP-fan1-L564R-loxM3</i> , <i>pso2::kanMX6</i> , <i>ura4D18</i> , <i>leu1-32</i> , <i>ade6-704</i>
AW1002	<i>h+</i> , <i>loxP-fan1-Q678A-loxM3</i> , <i>pso2::kanMX6</i> , <i>ura4D18</i> , <i>leu1-32</i> , <i>ade6-704</i>